Heat and Mass Transfer across Interfaces in Complex Nanogeometries

Øivind Wilhelmsen,* Thuat T. Trinh, Signe Kjelstrup, Titus S. van Erp, and Dick Bedeaux
Department of Chemistry, Norwegian University of Science and Technology, N-7491 Trondheim, Norway
(Received 21 October 2014; revised manuscript received 14 December 2014; published 12 February 2015)

Heat and mass transfer in nanodevices depends much on the geometry due to the strong influence of curvature on interfacial properties, such as the Kapitza resistance. We present a method which combines nonequilibrium square gradient theory and nonequilibrium molecular dynamics simulations to obtain the coefficients in a curvature expansion of the interface transfer coefficients. The expansion can be used directly to describe heat and mass transfer in complex nanogeometries. As examples of complex nanogeometries, we consider an oblate spheroidal droplet, a prolate spheroidal bubble, and a toroidal bubble. Depending on the sign and magnitude of the curvature, transfer is enhanced or reduced significantly. The presented method is applicable to many types of interfaces and substances, and we expect it to contribute to the understanding and design of future nanodevices.

DOI: 10.1103/PhysRevLett.114.065901 PACS numbers: 65.80.-g, 68.03.-g

The field of nanotechnology is rapidly developing, and demands knowledge of heat and mass transfer at the nanoscale [1]. A crucial difference between nano- and macroscopic systems is that interfaces constitute a significant part of the system. Experiments have shown a dependence of the thermal conductivity in nanoparticle suspensions on the size of the particles, where the resistance decreases for smaller particles [2,3]. Surprisingly, the nanoporous materials exhibit the opposite behavior with changing pore size [4]. It was hypothesized by Lervik *et al.*, that these effects could be explained by the interfacial curvature [5].

The interface is a considerable barrier to heat transfer, which is quantified by the Kapitza resistance. This resistance has been obtained from experiments and nonequilibrium molecular dynamics (NEMD) for a variety of interfaces and substances, e.g., vanadium-dioxide-air solid-gas interfaces [6], water-benzene liquid-liquid interfaces [7], and gold-water solid-liquid interfaces [8]. Few works have yet explored the curvature dependence of the Kapitza resistance, or other interface transfer coefficients, despite the striking importance in nanoscience [5,9]. Regardless of much scientific effort, the curvature dependence of even the surface tension is still poorly understood. The surface tension of a spherical droplet can be expanded to first order as $\gamma(\xi) = \gamma_0(1 - 2\tau/\xi)$, where ξ is the droplet radius and subscript 0 denotes the flat surface. The sign and magnitude of the first order correction, τ, known as the Tolman length, is still a hot topic of debate [10].

While surface tension is an equilibrium property, it is even more difficult to uncover the curvature dependence of interface transfer coefficients through molecular simulations, since these involve huge gradients in temperature or concentration. We present, in this Letter, a method which, for the first time, obtains the coefficients in a curvature expansion of interface transfer coefficients up to second order. The method gives the possibility to accurately describe transfer through interfaces of complex nanogeometries, and can help to understand complex nucleation processes and yet unexplained phenomena in nanoscience, or facilitate geometric design of nanodevices with desired properties. We use an oblate spheroidal droplet (M&M candy), a prolate spheroidal bubble (rugby ball), and a toroidal bubble (doughnut) to demonstrate the capabilities of the method in complex nanogeometries.

The method combines the atomistic details of NEMD simulations with the versatile mathematical formulation of square gradient theory (SGT), and is applicable to any multiphase system, like solid hydrates [11], crystals [12], or biological systems [13], for which the simple flat interface can be treated simultaneously with NEMD and SGT.

To obtain the coefficients in the curvature expansion, we use SGT, which is the first approximation to mass based density functional theory. A contribution is added to the Helmholtz energy proportional to the square of the density gradient [14]

$$F[\rho(\mathbf{r}), T] = \int d\mathbf{r}\left[f_{\text{eos}}(\rho(\mathbf{r}), T) + \frac{1}{2}\eta|\nabla\rho(\mathbf{r})|^2\right]. \quad (1)$$

Here, $\mathbf{r}$ is the position, f_{eos} is the equation of state value of the Helmholtz energy density in the homogeneous phases, ρ is the particle density, T is the temperature, and η is the influence parameter. Equilibrium density profiles through the interface region can be obtained by minimizing the Helmholtz energy, keeping the total number of particles constant. This gives a consistent set of thermodynamic variables which depend not only on the temperature and density, but also on spatial derivatives of the density. Moreover, we describe f_{eos} with a very accurate reference equation of state, and estimate η from the interaction potential [15]. With this model, we recently reproduced

the surface tension and Tolman length of the Lennard-Jones (LJ) fluid from molecular dynamics simulations [15]. This demonstrated that SGT was able to correctly account for the curvature dependence of interfacial properties.

SGT has also been extended to the nonequilibrium domain by including balance equations for momentum, mass, and energy [14]. For a flat surface, they reduce to a set of constant fluxes determined by the boundary conditions. For the particular case investigated in this Letter, the momentum balance gives a constant pressure tensor component perpendicular to the interface

$$p_\perp = p_{\mathrm{eos}}(T(z),\rho(z)) + \frac{\eta}{2}\left(\frac{\partial\rho(z)}{\partial z}\right)^2 - \eta\rho(z)\frac{\partial^2\rho(z)}{\partial z^2}, \tag{2}$$

where z is the coordinate perpendicular to the interface. Equivalent equations can be formulated for curvilinear geometries [16]. The energy balance gives a constant measurable heat flux, J'_q and the temperature through the interface region follows from:

$$\nabla\left(\frac{1}{T(\mathbf{r})}\right) = J'_q r_{qq}(\mathbf{r}). \tag{3}$$

Both $\eta = 4.9$ and p_{eos} are available from equilibrium simulations [15]. This implies that once an expression for the local resistivity r_{qq} is known, it is possible to numerically solve the coupled differential Eqs. (2) and (3) for a given set of boundary conditions. The solution gives the constants, $p_\perp$ and J'_q, but also temperature and density profiles and all properties that depend on these. Hence, r_{qq} represents the missing piece in the nonequilibrium-SGT formulation. In the bulk regions, it is connected to the thermal conductivity λ through $r_{qq} = (\lambda T^2)^{-1}$.

We will utilize atomistic simulations to obtain the functional form of r_{qq} across the interface in terms of temperature, density and density gradients from SGT.

The vapor-liquid interface of the Lennard-Jones fluid will be used as a benchmark example because it reproduces the properties of argon to a high accuracy, giving the possibility for testing results with both simulations and experiments. We used a truncated and shifted LJ potential with a large cutoff distance of 6σ and present results both for argon and in reduced units (LJ units). Results for argon were calculated using a well depth of $\epsilon/k_{\mathrm{B}} = 119.8$ K, a molecular diameter, $\sigma = 0.3405$ nm and a particle mass, $m = 6.69 \times 10^{-26}$ kg as parameters, where k_{B} is Boltzmann's constant.

To obtain information about r_{qq} in the interface region, we must consider a case which can be described simultaneously by NEMD and SGT. We used the well-established procedure from boundary driven NEMD simulations, where a liquid slab is located in the middle of a rectangular simulation volume with vapor phases on each side [17]. The simulation volume had the dimensions $\{L_x, L_y, L_z\} = \{20\sigma, 20\sigma, 100\sigma\}$. The temperature gradient was imposed in the z direction by thermostatting the region $|z/L_z| < 0.05$ to a low temperature, T_{cold}, and the regions $0.45 < |z/L_z| < 0.5$ to a high temperature, T_{hot}. Periodic boundary conditions were used, and the mass flux was zero. We found that nonequilibrium SGT reproduced the time-averaged temperature and density profiles from NEMD simulations along the entire coexistence line using the following local resistivity function as input:

$$r_{qq}(\mathbf{r}) = \frac{1}{\lambda(T,\rho)T(\mathbf{r})^2} + \left(\frac{\alpha(T)}{\rho(\mathbf{r})^2} + \frac{\beta(T)}{\rho(\mathbf{r})^4}\right)|\nabla\rho(\mathbf{r})|^2. \tag{4}$$

Here, $T_r = T/T_{\mathrm{c}}$ is the reduced temperature, and T_{c} is the critical temperature ($T_c = 1.29, 150.7$ K for the LJ fluid, argon). The second contribution to Eq. (4) gives a peak in the interface region, which because of the ρ^{-2} and ρ^{-4} prefactors is shifted towards the vapor phase compared to the equimolar surface. The resistivity profile is strongly asymmetric because most of the resistance is in the so-called "Knudsen layer" located closer to the vapor phase [18].

By comparing the temperature profiles from the nonequilibrium-SGT model to NEMD results, we obtained for the LJ fluid, $\alpha = 0.29T_r^{-5}$ and $\beta = 0.20T_r^{10}$. These parameters were independent of the truncation of the LJ potential for values larger than 3σ. Figure 1 shows nonequilibrium-SGT results in comparison with NEMD for one of the simulations that was used in the fitting procedure. Because of the interface resistance, a substantial temperature jump of the order of $0.1T_r$ developed across the interface. Both the size and location of the temperature jump from NEMD were reproduced to a good accuracy by the nonequilibrium-SGT model, as seen by comparing the solid and the dashed lines in Fig. 1. We expect Eq. (4) to work well for vapor-liquid interfaces, but anticipate the second contribution on

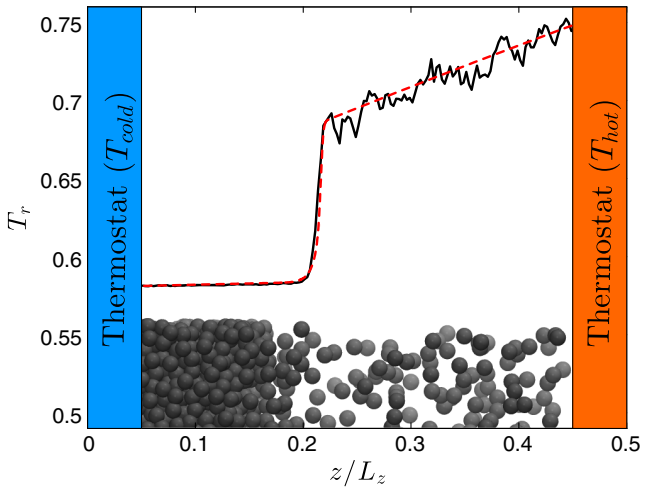

FIG. 1 (color online). Temperature profile from NEMD (solid line) and from nonequilibrium SGT (red dashed line).

the right-hand side to depend on the type of interface, and be different for, e.g., liquid-liquid, or gas-solid interfaces, since the interface resistance here is from a different physical mechanism than that of the Knudsen layer (acoustic mismatch). A similar approach, however, can be carried out for these systems to identify r_{qq}.

While SGT and NEMD give information about how the resistance changes locally through the interface region, a more practical quantity is the overall resistance of the interface. A consistent description of mass and heat transfer across interfaces in a single-component system can be obtained from nonequilibrium thermodynamics [19]

$$\frac{1}{T^{\mathrm{o}}} - \frac{1}{T^{\mathrm{i}}} = R_{qq} J_q'^{\mathrm{o}} + R^{\mathrm{o}}_{q\mu} J_\mu, \tag{5}$$

$$-\left(\frac{\mu^{\mathrm{o}}}{T^{\mathrm{o}}} - \frac{\mu^{\mathrm{i}}}{T^{\mathrm{i}}}\right) + h^{\mathrm{o}}\left(\frac{1}{T^{\mathrm{o}}} - \frac{1}{T^{\mathrm{i}}}\right) = R^{\mathrm{o}}_{\mu q} J_q'^{\mathrm{o}} + R^{\mathrm{o}}_{\mu\mu} J_\mu, \tag{6}$$

where the superscripts i and o indicate the values just inside or outside the interface, respectively. Furthermore, J_μ is the mass flux, μ is the chemical potential, h is the enthalpy, and R_{ij} are the overall interface transfer coefficients, known as interface resistivities. Following Onsager, the matrix of resistivities is symmetric, $R_{q\mu} = R_{\mu q}$, which gives only three independent resistivities. The Kapitza resistance, which frequently is reported from simulations and experiments, is given by $R_K = R_{qq}(T^s)^2$, where T^s is the surface temperature [19].

The link between the local description from SGT and the overall interface resistivities, R_{ij} is the integral relations. The validity of the integral relations has been verified by NEMD and nonequilibrium SGT [16,17]. The interface resistivities can be computed with the integral relations, using only equilibrium profiles through the interface. They are [14]

$$R_{ij}(\xi) = \mathfrak{h}_2^\xi \mathfrak{h}_3^\xi \int_{-\infty}^{\infty} dr \frac{\mathfrak{h}_1}{\mathfrak{h}_2 \mathfrak{h}_3} \phi_{ij}(r)^{\mathrm{ext}}. \tag{7}$$

Where again, ξ is the equimolar radius. Here, superscript ext means: $\phi(r)^{\mathrm{ext}} = \phi(r) - \phi^{\mathrm{i}}\Theta(\xi - r) - \phi^{\mathrm{o}}\Theta(r - \xi)$, where Θ, is the Heaviside function. Moreover, $\mathfrak{h}_1$, $\mathfrak{h}_2$, and $\mathfrak{h}_3$ are Lamé coefficients and superscript ξ means evaluated at the equimolar dividing surface. The Lamé coefficients are trivially 1 for a flat surface, and functions of the coordinate perpendicular to the interface for curved geometries. Equation (7) can also be used to calculate the interface resistivities for curved geometries, with the arguments, $\phi_{qq} = r_{qq}$, $\phi_{q\mu} = r_{qq}(h^{\mathrm{o}} - h)$, and $\phi_{\mu\mu} = r_{qq}(h^{\mathrm{o}} - h)^2$. Hence, all interface transfer coefficients $R_{qq}, R_{\mu\mu}$, and $R_{q\mu} = R_{\mu q}$ depend on the local resistivity r_{qq} expressed in Eq. (4). The interface resistivities of the flat interface, $R_{ij,0}$ are functions of the temperature only. In complex geometries, however, they also depend on the interface curvatures. This dependence can be expressed through the two principal curvatures, κ_1 and κ_2. An equivalent description which is used more commonly is obtained by using the total curvature, $H = \kappa_1 + \kappa_2$ and the Gaussian curvature, $K = \kappa_1\kappa_2$. We propose the following second order curvature expansion for the interface resistivities:

$$R_{ij}(H, K) = R_{ij,0}[1 + d_{ij}H + \nu_{ij}(d_{ij}H)^2 + \bar{\nu}_{ij}d_{ij}^2 K], \tag{8}$$

where $i, j = \{q, \mu\}$. The length, d_{ij}, gives the typical size of a droplet where curvature corrections become important, while ν and $\bar{\nu}$ are scalars. The curvature expansion in Eq. (8) becomes for a spherical (subscript s) and a cylindrical geometry (subscript c)

$$R_{ij,s}(\xi) = R_{ij,0}\left[1 + \frac{2d_{ij}}{\xi} + \frac{d_{ij}^2(4\nu_{ij} + \bar{\nu}_{ij})}{\xi^2}\right], \tag{9}$$

$$R_{ij,c}(\xi) = R_{ij,0}\left[1 + \frac{d_{ij}}{\xi} + \frac{d_{ij}^2\nu_{ij}}{\xi^2}\right]. \tag{10}$$

The square gradient model can now be solved for a spherical and a cylindrical geometry from negative curvatures (bubbles) to positive curvatures (droplets) and used together with the integral relations in Eq. (7) to obtain $R_{ij,s}(\xi)$ and $R_{ij,c}(\xi)$. This is illustrated by the solid line in Fig. 2. By performing a quadratic regression of the interface resistivities from negative curvatures to positive curvatures having relatively large radii to avoid higher order contributions, we obtain a second order polynomial in ξ^{-1} (red dashed line). The regression coefficients in the polynomial correspond to the prefactors in Eqs. (9) and (10). It turns out that it is sufficient to solve the square gradient model for a

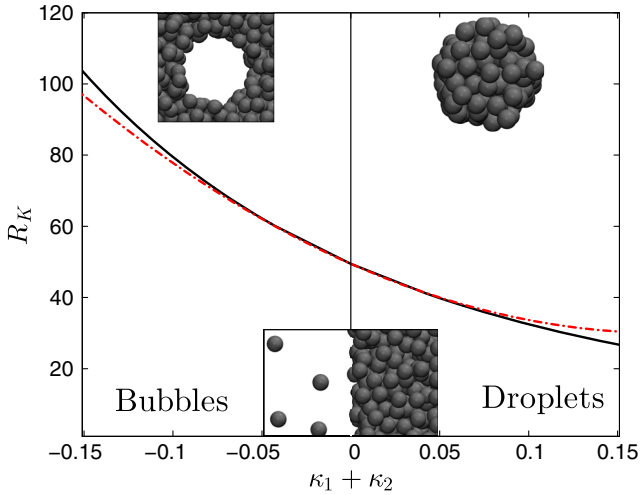

FIG. 2 (color online). The Kapitza resistance at $T_r = 0.58$ as a function of the total curvature in a spherical geometry, from the integral relations [Eq. (7), solid line], and the curvature expansion [Eq. (8), red dashed line].

TABLE I. The curvature expansion coefficients of the interface resistivities of the LJ fluid (argon) at $T_r = 0.58$.

	$R_{ij,0}$ (LJ)	$R_{ij,0}$ (argon)	d_{ij}/σ	ν_{ij}	$\bar{\nu}_{ij}$
R_{qq}	88.7	1.1×10^{-10} m^2 s/JK	−4.5	0.7	−0.2
$R_{q\mu}$	141.0	1.8×10^{-7} m^2 s/mol K	−2.7	0.9	−0.2
$R_{\mu\mu}$	359.6	4.5×10^{-4} Jm^2 s/mol^2 K	−2.1	0.9	−0.2
R_K	49.9	8.6×10^{-7} m^2 sK/J	−4.5	0.7	−0.2

flat interface, a cylindrical geometry, and a spherical geometry to obtain all the relevant coefficients in the curvature expansion, $R_{ij,0}$, d_{ij}, ν_{ij}, and $\bar{\nu}_{ij}$. We found the curvature expansion defined in Eq. (8) to predict the interface transfer coefficients to a good accuracy for geometries having dimensions of only a few nanometers, in a range where the Kapitza resistance can double in size (see Fig. 2).

Table I reports the coefficients in the curvature expansion of the interface resistivities of the vapor-liquid interface of the LJ fluid and argon at $T_r = 0.58$. A comprehensive analysis of their temperature and cutoff dependence will be presented in a future work.

The linear terms d_{ij} have the same dimension as the first order curvature correction of the surface tension, the Tolman length. The Tolman length of the LJ fluid was calculated from recent MD simulations to be -0.1σ [20], which is 45 times smaller in magnitude than, for instance, d_{qq}. It is clear that the interface resistivities depend much more strongly on curvature than the surface tension.

The coefficients in Table I give unique new insight into condensation or evaporation processes. MD simulations of nucleation, show that both the critical nucleus and cavity deviate from a spherical geometry [21,22]. The critical cluster of, for instance, water has an oblate spheroidal geometry [23], and recent work has shown that heat transfer may limit the growth [21]. This makes a curvature expansion of the interface resistivities useful to describe these processes accurately. There is, in principal, no restrictions to which geometries and shapes can be addressed with the curvature expansion in Eq. (8).

We shall use an oblate spheroidal droplet [M&M, Fig. 3a], a prolate spheroidal bubble [rugby ball, Fig. 3b], and a toroidal bubble [doughnut, Fig. 3c] as examples of complex nanogeometries. It is evident that curvature affects droplets and bubbles very differently. While the Kapitza resistance of the spheroidal droplet is smaller than that of a flat interface [Fig. 3a], the Kapitza resistance of the bubble is at some locations more than 2 times larger [Fig. 3b]. Another striking consequence of the large curvature dependence of the interface resistivities is that, even for relatively large droplets or bubbles as depicted in Fig. 3, the growth process must be fundamentally heterogeneous. It is surprising that, for droplets, transfer will be enhanced considerably at locations with high curvature [along equator in Fig. 3a]. For bubbles on the other hand, the resistance is largest at locations with high curvature [the end points in Fig. 3b]. Table I shows that the coefficients of heat transfer, mass transfer, and the coupling coefficient, all follow this behavior. Hence, fluctuations in shape enable the droplet or bubble to

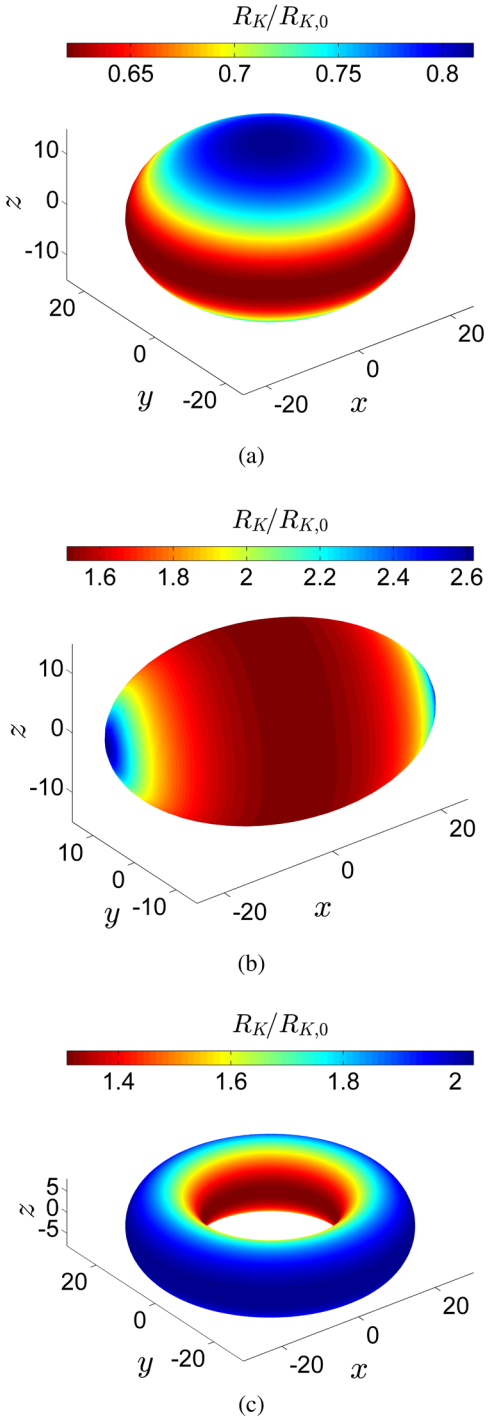

FIG. 3 (color online). The Kapitza resistance divided by the Kapitza resistance of the flat interface of argon at $T_r = 0.58$ of an (a) oblate spheroidal droplet, (b) prolate spheroidal bubble, (c) toroidal bubble. The spheroidal radii are 25 and 15, and the toroidal radii are 8 and 22 in reduced units.

enhance growth in some directions. This could have considerable implications on how the initial growth phase of nucleation should be understood. Videos showing how the Kapitza resistance changes with the shape, of a spheroidal bubble and a spheroidal droplet can be found in the Supplementary Material [24].

In nature, toroidal bubbles are induced by buoyancy or through cavitation near solid interfaces. Figure 3c shows that the Kapitza resistance of toroidal nanobubbles is very different at the outer and the inner surfaces.

In summary, we have presented a method for obtaining the curvature dependence of interface transfer coefficients, such as the Kapitza resistance, taking advantage of NEMD and SGT. The method has a wide range of applications and can be used to describe heat and mass transfer in complex nanogeometries. We believe that our method will be an excellent tool to deal with complex nucleation processes and for future studies aiming to unravel the previously mentioned puzzling behavior of nanoparticle suspensions and nanoporous materials. In addition, by mapping the curvature dependence of nanoparticles, pores, or other nanostructures, it may become possible to tailor the geometry to give the desired properties.

*oivind.wilhelmsen@ntnu.no

[1] F. Bresme and M. Oettel, Nanoparticles at fluid interfaces, J. Phys. Condens. Matter **19**, 413101 (2007).

[2] P. Keblinski, S. R. Phillpot, S. U. S. Choi, and J. A. Eastman, Mechanisms of heat flow in suspensions of nano-sized particles (nanofluids), Int. J. Heat Mass Transfer **45**, 855 (2002).

[3] H. E. Patel, S. K. Das, T. Sundararajan, A. S. Nair, B. George, and T. Pradeep, Thermal conductivities of naked and monolayer protected metal nanoparticle based nanofluids: Manifestation of anomalous enhancement and chemical effects, Appl. Phys. Lett. **83**, 2931 (2003).

[4] C. Bera, N. Mingo, and S. Volz, Marked Effects on Alloying on the Thermal Conductivity of Nanoporous Materials, Phys. Rev. Lett. **104**, 115502 (2010).

[5] A. Lervik, F. Bresme, and S. Kjelstrup, Heat transfer in soft nanoscale interfaces: the influence of interface curvature, Soft Matter **5**, 2407 (2009).

[6] C. Cheng, W. Fan, J. Cao, S.-G. Ryu, J. Ji, C. P. Grigoropoulos, and J. Wu, Heat Transfer across the Interface between Nanoscale Solids and Gas, ACS Nano **5**, 10102 (2011).

[7] H. A. Patel, S. Garde, and P. Keblinski, Thermal resistance of nanoscopic liquid-liquid interfaces: dependence on chemistry and molecular architecture, Nano Lett. **5**, 2225 (2005).

[8] Z. Ge, D. G. Cahill, and P. V. Braun, Thermal Conductance of Hydrophilic and Hydrophobic Interfaces, Phys. Rev. Lett. **96**, 186101 (2006).

[9] Z. Liang, K. Sasikumar, and P. Keblinski, Thermal Transport across a Substrate-Thin-Film Interface: Effects of Film Thickness and Surface Roughness, Phys. Rev. Lett. **113**, 065901 (2014).

[10] Y. A. Lei, T. Bykov, S. Yoo, and X. C. Zeng, The Tolman Length: Is it positive or negative?, J. Am. Chem. Soc. **127**, 15346 (2005).

[11] B. Kvamme, A. Graue, E. Aspenes, T. Kuznetsova, L. Gránásy, G. Tóth, T. Pusztai, and G. Tegze, Kinetics of solid hydrate formation by carbon dioxide: Phase field theory of hydrate nucleation and magnetic resonance imaging, Phys. Chem. Chem. Phys. **6**, 2327 (2004).

[12] L. Gránásy, T. Pusztai, T. Börzsönyi, J. A. Warren, and J. F. Douglas, A general mechanism of polycrystalline growth, Nature (London) **3**, 645 (2004).

[13] T. Biben, K. Kassner, and C. Misbah, Phase-field approach to three-dimensional vesicle dynamics, Phys. Rev. E **72**, 041921 (2005).

[14] K. S. Glavatskiy and D. Bedeaux, Resistances for heat and mass transfer through a liquid-vapor interface in a binary mixture, J. Chem. Phys. **133**, 234501 (2010).

[15] Ø. Wilhelmsen, D. Bedeaux, and D. Reguera, Tolman Length and Rigidity Constants of the Lennard-Jones fluid, [J. Chem. Phys. (to be published)].

[16] Ø. Wilhelmsen, D. Bedeaux, and S. Kjelstrup, Heat and mass transfer through interfaces of nanosized bubbles/droplets: the influence of interface curvature, Phys. Chem. Chem. Phys. **16**, 10573 (2014).

[17] J. M. Simon, D. Bedeaux, S. Kjelstrup, J. Xu, and E. Johannessen, Interface film resistivities for heat and mass transfers-integral relations verified by non-equilibrium molecular dynamics, J. Phys. Chem. B **110**, 18528 (2006).

[18] M. Bond and H. Struchtrup, Mean evaporation and condensation coefficients based on energy dependent condensation probability, Phys. Rev. E **70**, 061605 (2004).

[19] S. Kjelstrup and D. Bedeaux, *Non-Equilibrium Thermodynamics of Heterogeneous Systems* (World Scientific, Singapore, 2008).

[20] A. E. van Giessen and E. M. Blokhuis, Direct determination of the Tolman length from the bulk pressures of liquid drops via molecular dynamics simulations, J. Chem. Phys. **131**, 164705 (2009).

[21] R. Holyst and M. Litniewski, Heat Transfer at the Nanoscale: Evaporation of Nanodroplets, Phys. Rev. Lett. **100**, 055701 (2008).

[22] Z.-J. Wang, C. Valeriani, and D. Frenkel, Homogeneous bubble nucleation driven by local hot spots: A molecular dynamics study, J. Phys. Chem. B **113**, 3776 (2009).

[23] M. N. Joswiak, N. Duff, M. F. Doherty, and B. Peters, Size-Dependent Surface Free Energy and Tolman-Corrected Droplet Nucleation of TIP4P/2005 Water, J. Phys. Chem. Lett. **4**, 4267 (2013).

[24] See Supplemental Material at http://link.aps.org/supplemental/10.1103/PhysRevLett.114.065901 for videos of the shape-dependent Kapitza resistance of a nanodroplet and a nanobubble.